

RESEARCH ARTICLE

Mechanism of signal uncertainty generation for laser-induced breakdown spectroscopy

Yang-Ting Fu¹, Wei-Lun Gu¹, Zong-Yu Hou¹, Sher Afgan Muhammed¹, Tian-Qi Li¹, Yun Wang², Zhe Wang^{1,†}

¹State Key Lab of Power Systems, International Joint Laboratory on Low Carbon Clean Energy, Innovation, Department of Energy and Power Engineering, Tsinghua University, Beijing 100084, China

²Renewable Energy Resources Laboratory (RERL) & National Fuel Cell Research Center, Department of Mechanical and Aerospace Engineering, The University of California, Irvine, CA 92697-3975, USA

Corresponding author. E-mail: †zhewang@tsinghua.edu.cn

Received August 30, 2020; accepted September 20, 2020

Relatively large measurement uncertainty severely hindered wide application for laser-induced breakdown spectroscopy (LIBS), therefore it is of great importance to understand the mechanism of signal uncertainty generation, including initiation and propagation. It has been found that the fluctuation of plasma morphology was the main reason for signal uncertainty. However, it still remains unclear what mechanism leads to laser-induced plasma morphology fluctuation. In the present work, we employed three fast-imaging cameras to capture three successive plasma images from a same laser-induced Titanium alloy plasma, which enables us to understand more clearly of the plasma evolution process especially for the early plasma evolution stage when plasma and surrounding gases interact drastically. Seen from the images, the plasma experienced an increasing morphological fluctuation as delay time increased, transforming from a “stable plasma” before the delay time of 100 ns to a “fluctuating plasma” after the delay time of 300 ns. Notably, the frontier part of plasma showed a significant downward motion from the delay time of 150 ns to 200 ns and crashed with the lower part of the plasma, making the plasma flatter and later even splitting the plasma into two parts, which was considered as a critical process for the transformation of “stable plasma” to “unstable plasma”. By calculating the correlation coefficient of plasma image pairs at successive delay times, it was found that the higher the similarity between two plasma at early stage, the more similar at later stage; this implied that the tiny plasma fluctuation earlier than the critical delay time (150–200 ns) was amplified, causing a large plasma fluctuation at the later stage as well as LIBS measurement uncertainty. The initiation of slight fluctuation was linked with Rayleigh–Taylor Instability (RTI) due to the drastic material interpenetration at the plasma–ambient gas interface at earlier stage (before 50 ns). That is, the uncertainty generation of LIBS was proposed as: plasma morphology fluctuation was inevitably triggered by RTI at the early stage and the tiny fluctuation was amplified by the back pressed downward process of plasma frontier material, leading to severe morphology fluctuation as well as LIBS signal uncertainty.

Keywords LIBS, laser-induced breakdown spectroscopy, signal uncertainty, Rayleigh–Taylor instability

1 Introduction

Laser-induced breakdown spectroscopy (LIBS), as a rapid analytical method for elemental analysis, has been widely applied in various industrial applications [1–4]. Compared with conventional atomic emission spectroscopy (AES) methods such as ICP-AES, LIBS has its distinct advan-

tages of online/in-situ and minimal sample preparation etc., earning LIBS technique with “future superstar” in the analytical field [5]. However, the biggest drawback of LIBS is its relatively low measurement repeatability [2, 6–8]. Without solving the low measurement repeatability problem, the complete commercialization of the LIBS technique as a robust quantitative analysis method will be unattainable. The key to solve the problem is to understand the mechanism of the signal uncertainty generation and propagation.

Extensive efforts have been made in the LIBS community to find methods to reduce the LIBS signal fluctuation.

*This article can also be found at <http://journal.hep.com.cn/fop/EN/10.1007/s11467-020-1006-0>.



tuations using both experimental methods and theoretical simulations or calculations. Processes or factors such as the uncontrollable laser-matter interactions [1, 9], the plasma shielding effects [10, 11] the temporal and spatial evolution of a non-uniform plasma and the rough sample surface [12], will all bring uncertainties to the actual spectral signals received by the detectors. Experimental methods such as cavity confinement [13–15], magnetic confinement [16, 17], and long-short dual pulse configuration [18] have been applied to successfully enhance the LIBS signal stability. Therefore, it was more and more clear that the relative low measurement repeatability of LIBS due to its large shot-to-shot signal fluctuation originated from laser-induced plasma morphology fluctuation due to the complex physical processes during the laser-induced plasma generation and evolution [14, 15, 19–23]. However, there is still very little work understanding the mechanism leading to large plasma morphology fluctuations as well as measurement uncertainty.

Previously, we have investigated the origins of the signal uncertainties from the perspective of plasma parameter fluctuation, and confirmed that the fluctuation of total number density was the pivotal factor affecting the LIBS spectral signal uncertainty [19]. Considering that majority of the spectral emissions collected by the optics system comes from a small core area of the plasma [24], and the fluctuation of the total number density is closely related to the fluctuation of the plasma morphology, or the fluctuation of the spatial distributions of the plasma image intensities [13], it would be very necessary to understand the key process during the plasma evolution that brings the plasma morphological fluctuation. By understanding this key process bringing the plasma morphological fluctuations, we should be able to find more practical and effective methods to control the process and therefore reduce the LIBS signal fluctuations.

In this paper, employing the continuous fast photography setup, we mainly focus on the temporal plasma morphological evolution and fluctuations. In addition, to clearly analyze the morphology evolution of a laser-induced plasma, we employed three CMOS cameras controlled by one digital delay generator for capturing the plasma images from the same field-of-view. Special attention was paid to the critical delay times when the plasma experienced a major morphological transition. The purpose of this study was to find the mechanisms that bring the LIBS signal fluctuation based on the plasma morphology stability analysis, to find more effective ways to control the plasma to increase the LIBS measurement repeatability.

2 Experimental details

A schematic diagram of the setup is shown in Fig. 1. An Nd:YAG laser (Q-smart 100, Quantel, France), operated

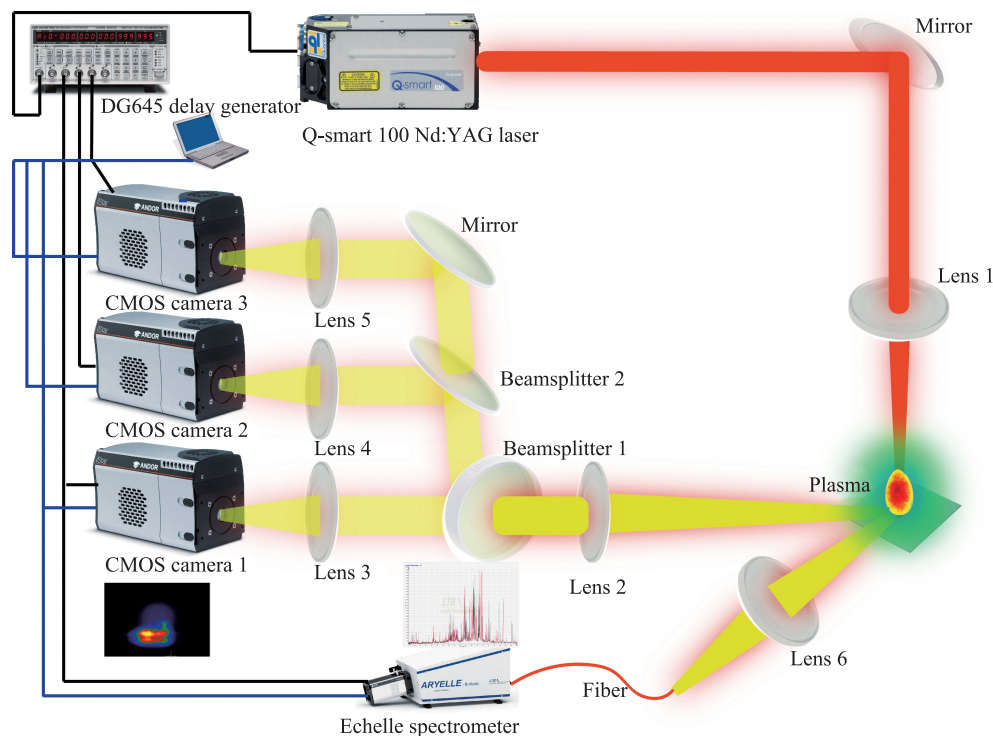


Fig. 1 Experimental setup used in this study. Three sCMOS cameras were employed to capture continuous plasma images from one plasma. An Echelle spectrometer was used to take temporally-resolved spectra of the laser-induced plasma.

in the fundamental wavelength of 1064 nm, was used in this experiment as the laser source. The laser energy was set to be 100 mJ per pulse, with a pulse width of 4 ns and a repetition rate of 1 Hz. The laser beam was focused onto the sample by a fused silica lens (Lens1) with a focal length of 150 mm to generate laser-induced plasma. The focal point was adjusted to be 2 mm below the sample surface, making the spot size around 300 μm . The plasma emission was firstly collimated by an $f = 100$ mm fused silica lens (Lens 2), successively passed and reflected by two beam splitters, (Beamsplitter 1 and Beamsplitter 2), generating three collimated emission beams, then the three collimated emission beams were focused by three identical $f = 75$ mm fused silica lenses (Lens 3, Lens 4, Lens 5) on the imaging focal planes of three gated sCMOS cameras (iStar sCMOS, Andor, UK) for simultaneous plasma image acquisition. The relative delay times between the laser output and the three cameras were controlled by a digital delay generator (DG645, Stanford Research System, USA). With this configuration, the three cameras would be able to observe the same fast-evolving laser-induced plasma from the same field-of-view simulta-

neously, and by changing the relative gate delays of each camera, three consecutive images can be obtained from one plasma and the inter-image delays can be changed discretionarily. Getting consecutive plasma evolution images from one plasma is important in our current study, as our goal is to investigate the possible critical moment bringing the signal fluctuation of the plasma. Thus, plasma images before, at and after the possible critical moment from the same plasma can be taken simultaneously and are highly correlated. In this work, the gate delays of three cameras were changed between 10 ns to a few μs , with each gate width adjusted correspondingly according to the relative image pixel intensity. Various neutral density optical filters were implemented before the incident windows of the cameras to avoid over-exposure. Besides, an Echelle spectrometer coupled with a fast-gated ICCD (Aryelle Butterfly, LTB, Germany) was also implemented to collect temporally-resolved spectra of laser-induced plasma.

A standard titanium alloy sample (TC4-4, 88.2% Ti, 4.46% V, 6.48% Fe) was used in this study. The sample was placed on a manually x - y axis movable platform. After each laser shot, the sample was moved to a fresh spot

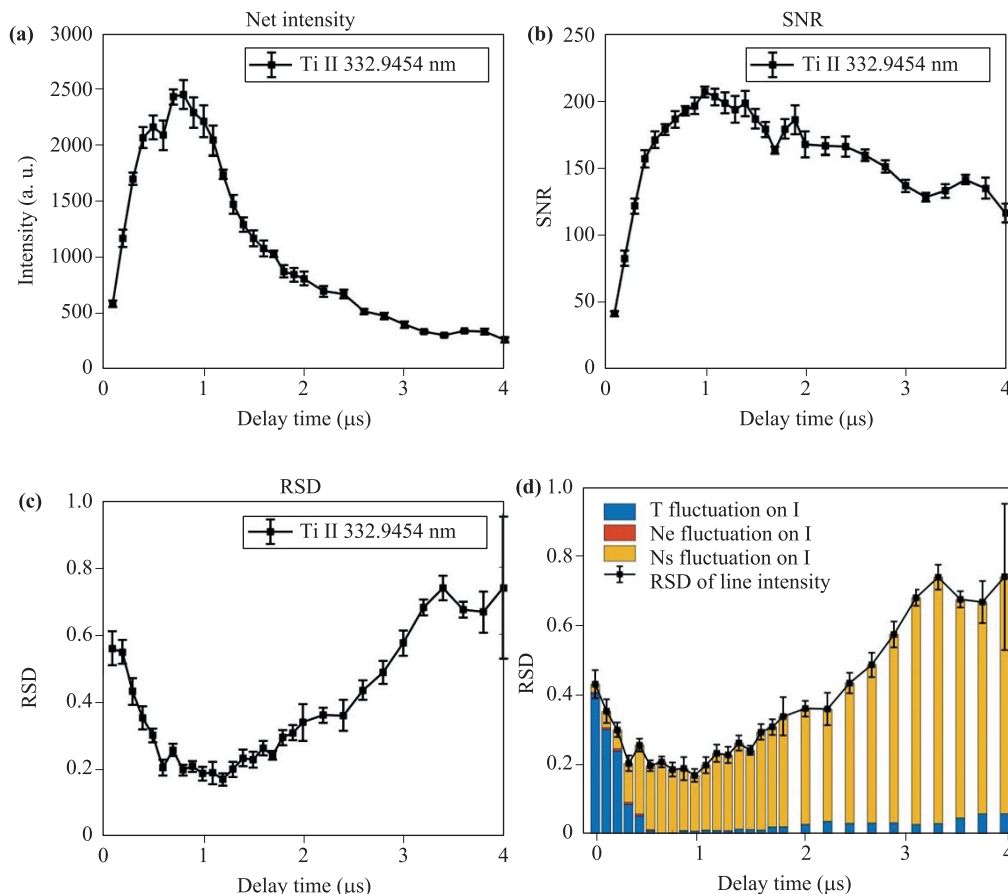


Fig. 2 The temporal evolution of Ti II 332.945 nm (a) net intensity, (b) SNR, (c) RSD, and (d) relative contribution on total RSD from the fluctuation of plasma parameters, namely, plasma temperature T , electron density n_e , and total number density of the measured element n_s . The error bars in the figures represent the standard deviation of the calculated data from 5 repeated times of the experiment.

to avoid repetitive striking on the same spot. Three successive gate delays with appropriate gate widths for three cameras were employed to acquire three plasma images in the time range of 10 ns to a few μs . Under each delay setting, 20 laser shots were fired, generating 60 plasma images in total (20 images from each camera). Plasma images as well as raw data matrix were processed in Matlab software for further calculation and analysis.

Temporal-resolved spectra was taken to show the temporal evolution of line intensity, signal-to-noise ratio (SNR) and relative standard deviation (RSD). The delay times of the spectra acquisition were set in the range of 0.1 to 4 μs and the gate width was fixed as 100 ns. Ti ion (Ti II) spectra from the laser-induced Ti alloy plasma were dominant in the investigated time windows. Thus, a typical Ti II line centered at 332.9454 nm was used for the spectral analysis.

3 Results and discussion

3.1 Temporal evolution of plasma stability

We started the analysis from the temporal evolution of spectra intensity, SNR and RSD and the morphological observation of the laser-induced Ti alloy plasma at different delay times, as shown in Figs. 2(a)–(c). Ti II 332.9454 nm line net intensity and SNR increases as delay time increases within 1 μs and gradually decreases after 1 μs . The spectral intensity fluctuation, expressed by the shot-to-shot RSD, had the trend of decreasing RSD within 1 μs and subsequently increasing after 1 μs . From the spectroscopic point of view, an optimized time window for spectra acquisition lies around the delay time of 1 μs . We also calculated the relative contribution of fluctuations of three plasma parameters, namely, plasma temperature T , electron density n_e and total number density of species n_s , on the spectral signal RSD of Ti II 332.9454 nm line. The result was presented in Fig. 2(d). The methodology of the calculation was described in reference [19]. Seen from Fig. 2(d), also, the fluctuation of line intensity was mainly contributed by temperature fluctuation at early stage (before 500 ns) and by total number density fluctuations at later stage (after 500 ns); and the earlier the delay time, the less the fluctuation of total number density contribution to total RSD seen from Fig. 2(d). Looking deeper into the results, it was found that earlier in 300 ns, the fluctuation of total number density, which was mostly due to plasma morphology variation, started to contribute more and more to total RSD. That means, something happened before 300 ns to make the plasma morphology unrepeatable.

To further study the early-stage plasma emission fluctuation, we mainly focused on the plasma morphological fluctuation by analyzing the temporally-resolved images. Figure 3 presented the temporal evolution of the plasma

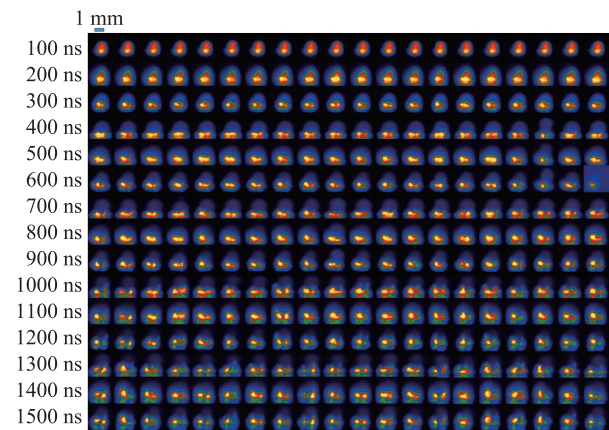


Fig. 3 Temporal evolution of laser-induced Ti alloy plasma morphology fluctuations.

from 100 ns to 1500 ns. At each delay time, 20 plasma images were obtained from 20 laser shots for plasma repeatability analysis. An immediate conclusion drawn by examining the temporal evolution of plasma morphology is that plasma generally experienced a deteriorating fluctuation as delay time increases. From Fig. 3, the 20 plasmas from 100 ns were almost identical to each other, while after a few hundreds of nanoseconds they showed a significant discrepancy from each other. Another interesting phenomenon from Fig. 3 is that the plasma started with a near hemispherical shape (~ 100 ns) while the upper part of the plasma immediately dashed down to the surface of the sample in the next 100 to 200 ns. The plasma was in a compressed shape for about 600 ns and ultimately split into two halves (~ 1000 ns and above). The first three rows in Fig. 3 revealed that the most significant morphological change took place and sensible plasma morphological fluctuation started to appear somewhere between 100 ns and 300 ns.

This can be further clarified by checking the correlation coefficient, which was applied to quantify the similarity between two images at the same delay time, at different delay times. The correlation coefficient was defined to describe the similarity of two plasma morphological images. For two arbitrary plasma images from the same delay time, the correlation coefficient was calculated as follows: i) choose a rectangular area where the major part of the plasma occupies in the plasma intensity matrix as the matrix for correlation coefficient analysis. The size of the area is chosen empirically which includes all the pixels of which the intensity is higher than $1/e$ of the maximum intensity, and contains as fewer background intensity pixels as possible. It is important to note that the size of the matrix from all plasma images of all delay times shall remain consistent for significative comparison. ii) Regarding the two chosen plasma intensity matrix A and B , each of with has m rows and n columns, for the two column vectors from the corresponding column positions

of the two matrixes, calculate the correlation coefficient of the two vectors. The final correlation coefficient $Corr$ is the average value of the correlation coefficients from the n column vector pairs, described in Eq. (1), where $\mathbf{a}_j = (a_{1j}, a_{2j}, \dots, a_{mj})^T$ and $\mathbf{b}_j = (b_{1j}, b_{2j}, \dots, b_{mj})^T$ are the two column vectors from matrix A and B at column j . $corr(\mathbf{a}_j, \mathbf{b}_j)$ is the correlation coefficient of the two vectors \mathbf{a}_j and \mathbf{b}_j ,

$$Corr = \frac{1}{n} \sum_{j=1}^n corr(\mathbf{a}_j, \mathbf{b}_j). \tag{1}$$

The temporal evolution of the plasma morphology fluctuation can be seen from the plasma pair correlation coefficients at different times, as shown in Fig. 4. The circle in the Fig. 4 clearly showed an abrupt drop of the correlation coefficient between the delay time of 150 ns and 200 ns, indicating the drastic plasma morphological transition. In this time period, the plasma experienced a transition from relatively “stable” to “unstable”.

During this time frame, previous studies [25, 26] suggested internal shockwaves were bouncing back and forth inside laser-induced plasma within a few hundreds of nanoseconds from the plasma initiation, creating a more homogeneous plasma from the process of internal shockwave sweeping the plasma particles after a few bouncing periods. We can see that from the plasma morphological evolution, the evidence of internal shockwave effect was not so clear. Thinking of the high plasma temperature, the excitation temperature would be somehow above 20 000 K at this time, and the sonic speed in the plasma would be roughly estimated to be as high as 2.50 km/s according to the formula of ion speed of sound $c = \sqrt{\gamma Z k T_e / m_i}$, where γ is the adiabatic index, Z is the charge state, k

is the Boltzmann constant, T_e is the plasma temperature and m_i is the ion mass. The movement speed of the upper part of the plasma around this time can also be estimated to be in the range of 2 to 5 km/s by measuring the positions of plasma frontiers at different delay times from the images, which was in the same magnitude of very early stage plasma and shockwave expansion speed as well as to sonic speed inside the plasma. That is, the mobility of the elements inside the plasma to carry the force/energy to balance the external shockwave is high enough, and there is not necessary to form internal shockwave to transfer the back-pressed energy from external shockwave. In addition, the evolution of morphology most possibly implied a mass transfer of plasma materials instead of only transferring energy through internal shockwave from delay time of 150 ns to 200 ns. In another word, during this critical time period (delay time 150–200 ns), there would exist the phenomenon that the frontier of the plasma dash-down back to the center of the plasma. Also, previous studies have indicated that the propagation of external shockwave and the interaction of expanding plasma and external shockwave were linked to the non-uniform spatial distribution of spectral intensity, as well as shot-to-shot signal fluctuations [27–30]. The dash-down process should be resulted from the generation of external shockwave at this moment and once such a high-speed material crashed with the lower part, very tiny fluctuation existed before the crashing would greatly affect the plasma morphology afterwards.

This deduction was further supported by the plasma images taken at delay time after 1000 ns where plasma splitting was seen and internal shockwave seems to be very hard to generating the splitting. In addition, we noticed that only from plasma image, it cannot be absolutely right to make such a conclusion since the image emission will also depend on the plasma temperature in addition to plasma material distribution, and there needs more spatial resolved spectral information to further confirm this assumption. Later in this work, it was further deduced that the bounced-back mass transfer could be the fundamental reason leading to large signal fluctuation for LIBS measurement.

3.2 Plasmas image evolution near the “critical time”

As mentioned above, it was implied that the dash-down process of the plasma frontier material somewhere between 100–300 ns may be the main reason splitting the plasma and bringing the morphological fluctuation. To have a clearer and deeper understanding of the critical process generating the plasma morphology fluctuation, special attention was paid to the plasma morphology around this period. Especially, to find the linkage of the plasma morphology, three cameras were set to catch the plasma image from a same plasma going through this period.

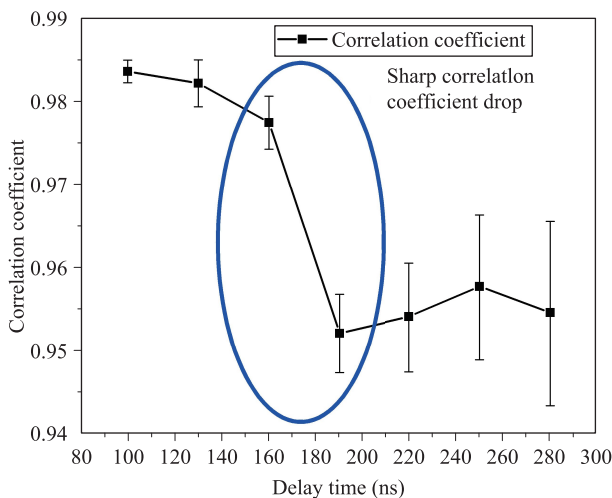


Fig. 4 Average correlation coefficients of plasma image pairs at early stage of plasma evolution. The error bars in the figures represent the standard deviation of the calculated data from 5 repeated times of the experiment.

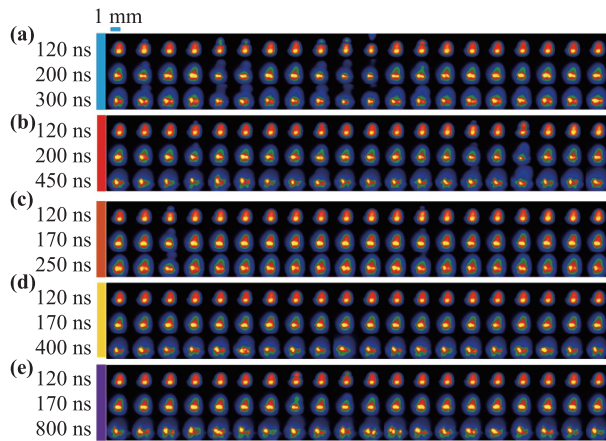


Fig. 5 Plasma morphological evolution around the “critical times”: (a–e) shows five different time setting regimes for three cameras for consecutive image acquisition.

In Fig. 5(a) and Fig. 5(b), the delay times of the first two cameras were fixed as 120 ns and 200 ns while the delay times of the third camera were set as 300 ns and 450 ns, respectively. In Figs. 5(c)–(e), the delay times of the first two cameras were fixed as 120 ns and 170 ns, while the delay times of the third camera were changed from 250 ns to 800 ns. From Figs. 5(a)–(e), the critical moment of plasma transforming from the “stable” to “unstable” status should be somewhere around 170 ns, consistent with the results from Fig. 4 where the correlation coefficient dropped drastically between 150 ns and 200 ns. Around this critical time, as mentioned above, the back-pressed frontier part of plasma crashed with the lower part of the plasma and started to flatter and even split the plasma. This dash-down and crash process is critical to the emergence of the plasma fluctuation at later stage.

A natural idea would be comparing the correlation coefficients of plasma pairs from three consecutive delay times. Since the three consecutive images were taken from a same plasma in Fig. 5, we are able to look deeper into the morphology evolution by calculating the correlation coefficient among these images. It was very interesting to see how “smaller fluctuation” at early stage of the plasma evolution evolves to much “larger fluctuation” at later stage of the plasma. In Fig. 5, the delay times of three cameras were set as 120 ns, 200 ns, and 450 ns, respectively. The correlation coefficients of the plasma images from each delay time were calculated pairwise, then the plasma pairs with the largest correlation coefficient were singled out, as the “most identical plasma pairs”. Figure 6 also showed the correlation coefficients of all the plasma pairs which contained at least one of the singled out the “most identical plasma pair”. At a delay time of 120 ns, all the investigated plasma pairs were almost identical with the correlation coefficients close to 0.99, and the fluctuation of the correlation coefficients was small between different plasma pairs, confirming the plasma images were quite identical

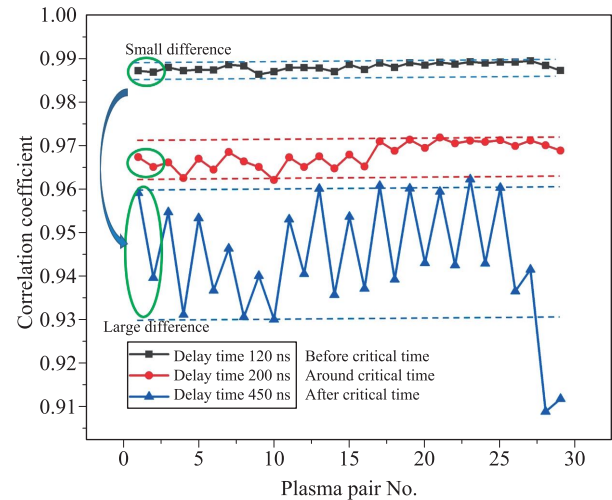


Fig. 6 Comparison of correlation coefficients from different plasma pairs at three different delay times. The dash lines and the circles at different delay times indicate smaller fluctuations before critical time will be amplified to larger fluctuations during the critical time.

with slight difference. At a delay time of 200 ns, the fluctuation of the correlation coefficients increased between different plasma pairs, and further at delay time of 450 ns, with the fluctuation of correlation coefficients became even more drastic, which was consistent with previous conclusion that the dash-down process and crashing process amplifying the fluctuation. Further analyzing the coefficient pairs, it was found that the fluctuation of the correlation coefficients from different delay times of a same plasma followed the same pattern, merely with the amplitudes of the fluctuation increased with delay time. From the plasma morphological perspective, it meant that a small morphological fluctuation at early delay time, i.e., 120 ns, after going through the “plasma dashing downward and crashing” process, the fluctuation would amplify itself, causing more severe fluctuation at later delay times, i.e., 200 ns and 450 ns. Combining the results drawn from Fig. 5 and Fig. 6, one could conclude that during the critical time when the upper part of the plasma dashed downwards to split the Ti plasma, the plasma experienced the transition from “stable” to “unstable”, and the small plasma morphological fluctuations before the critical time would amplify itself during this critical time, bringing more severe plasma morphological fluctuations at later delay times.

3.3 Further discussion

Rayleigh–Taylor instability (RTI) has been extensively discussed in the context of laser-induced plasma instability and it was normally applied to explain phenomena like ripple-shaped perturbation on the plasma front [31] and plasma stratification [32] at low pressure. It was speculated that the mechanism leading to the plasma instabil-

ity would be to attribute to the growth of RTI. However, since the necessary condition for RTI to occur in laser-induced plasmas is that the density of plasma should be higher than that of the ambient gas [31], to have significant RTI in laser-induced plasma, either the ambient pressure should remain significantly low, or atmosphere with low density such as He should be used [33], or the detection window should be restricted to very early stage of the plasma when the plasma density is high enough. That is, a big concern is that so far most works on RTI in laser-induced plasmas were conducted under low ambient pressure, either theoretically or experimentally [31–37] and it may not be the same case in ambient gas since of the density difference would be not favorable for RTI. In the present work, we attempted to extend the RTI discussion to our case at atmospheric pressure to find what extent RTI will affect plasma morphology change.

At very early stage of plasma expansion when plasma expands into ambient gas supersonically, due to the density differences between plasma and ambient gas, drastic material interpenetration takes place at the plasma-ambient gas interface, causing the RTI phenomenon. Although in the situation of laser-induced plasma, it was clearly in compressible fluid regime, according to the theoretical analysis of Kull *et al.* [38], the compressibility effects often only brings a small correction in the instability growth rate of the RT instability. Therefore, in the present work, we applied the RTI theory in the incompressible regime to obtain the time when RTI grows vigorously as a rough estimate [38]. Besides, various studies previously have successfully used the snow-plow model to predict the growth of the Rayleigh–Taylor instability at the plasma-gas interface with agreeable precision [31, 37], furthering supporting our choice in estimating the RTI strongest time.

In the RTI regime for incompressible fluids, the amplitude of a sinusoidal perturbation grows exponentially as $\exp(nt)$, where

$$n = \sqrt{ak \cdot At}, \quad (2)$$

$$At = \frac{\rho_b - \rho_p}{\rho_b + \rho_p}. \quad (3)$$

Here, a is the acceleration of the plasma front, k is the wavenumber of the sinusoidal perturbation, and At , Atwood number, describes the density dependence of RTI. ρ_b and ρ_p are the density of the ambient gas and the plasma, respectively. From the RTI theory, the interface becomes unstable if the density of plasma is higher than that of the ambient gas. As mentioned in literature [31, 32], the growth of instability occurs in the maximum deceleration region. To estimate the corresponding time, we solve the momentum conservation equation

$$M_0 u_0 = \left(M_0 + \frac{2}{3} \pi R^3 \rho_b \right) u \quad (4)$$

with the assumption of a homogeneous plasma and semi-spherical expansion, where $M_0 u_0$ is the initial momentum of the plasma, R is the radius of the plasma, and $u = dR/dt$ is the velocity of the plasma front. The solution of this equation yields

$$R = \left(\frac{3M_0}{7\pi\rho_b} \right)^{\frac{1}{3}}, \quad (5)$$

where R is the radius of the plasma with maximum deceleration. With $M_0 \approx 10^{-6}$ g as estimated from a typical laser-induced plasma ablated mass, $\rho_b = 1.29$ kg/m³, R is estimated to be 0.47 mm. From early stage plasma images, plasma with this radius occurs in the range of 10 to 50 ns [15]. That is, at atmospheric pressure, RTI seems to only occur at ultra-early stage of the plasma evolution. Of course, this is only an approximate estimation with possible large errors, but it gives an overall indication that under atmospheric environment, RTI might only occur at very early stage of the plasma evolution. The result was comparable with literature [36], in which Rifai *et al.* theoretically evaluated the RTI occurrence time in Ar atmosphere with 0.1 atm pressure and revealed that RTI only existed before 3 ns. As density of air in 1 atm is higher than that of Ar in 0.1 atm, we would estimate that RTI should also only happen in the very beginning of the plasma evolution. Actually, except for the very early stage, laser-induced plasma at atmospheric pressure usually has smaller density compared to the ambient atmosphere [39], which is contrary to the condition required for RTI to keep existing. That is, the morphology instability we watched in our experiment after 150 ns cannot be attributed to RTI.

Although RTI was regarded not to be the reason for laser-induced plasma morphology fluctuation, it may still play an important role in generation large morphology fluctuations: RTI at the ultra-early stage of the plasma expansion could “bury a seed” of instability at the interface, bringing the initial asymmetric perturbation which will be amplified in the later stage. As described in previous section, if the plasma was more similar in early stage (before 100 ns), the morphology would be also more similar in later stage. That is, if there was no disturbance in ultra-early plasma evolution, the plasma morphology would still be repeatable even there is an amplification process afterwards. According to the estimation above, RTI occurred most drastically around 10–50 ns and was diminished due to plasma density decrease below ambient gas very soon after, but the disturbance it caused may have generated asymmetric velocity and slightly variation in plasma morphology. This is consistent with what we have observed in our experiment, there was slight difference existed for plasma morphology at delay time 100 ns, which may be generated due to RTI. In addition, due to surface roughness and imperfect laser-sample alignment, there would also be slightly different in laser-sample interaction as well as slight plasma morphology difference. Overall, there is

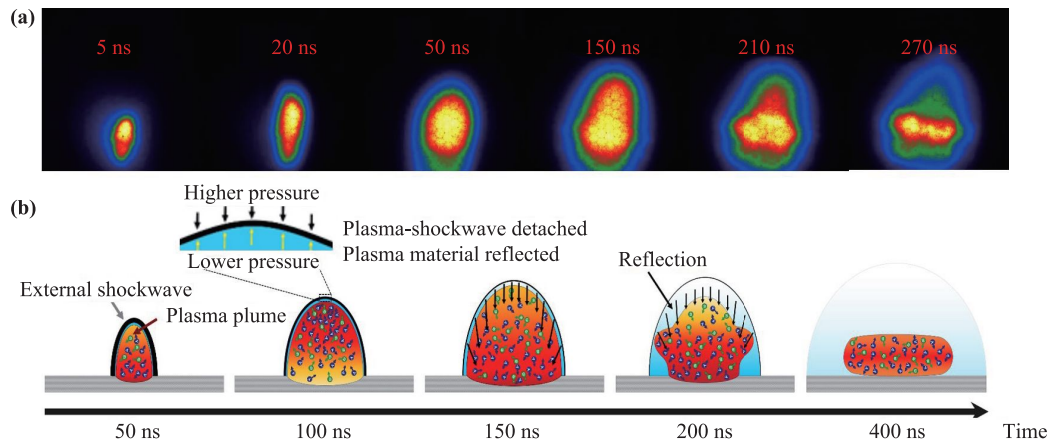


Fig. 7 (a) A stream of plasma images at early stage of plasma evolution, showing the plasma material migration and collision process. (b) The diagram of plasma plume and external shockwave evolution.

inevitably fluctuation seed existed in plasma evolution at the very early stage due to RTI and surface roughness.

Combining all the discussion above, the mechanism of LIBS uncertainty generation was proposed: due to RTI and surface roughness, there inevitably existed morphological fluctuation when plasma was initiated and expanded, and the small morphological fluctuation was amplified by the thereafter frontier material dash-down and crash with lower part of the plasma, therefore generating large LIBS measurement uncertainty. What remained to be explained now is what mechanism lead to the dash-down process. It was noticed that in earlier work, the dash-down process may come from the pressure gradient caused by the fast expansion of the plasma in the plasma front [40, 41]. In the present work, we proposed the following more detailed mechanism by analyzing the mixing and expansion process of plasma in ambient gas to better address the dash-down movement of the frontier plasma material and the time coincidence of shockwave generation and dash-down process of the frontier plasma.

The plasma materials from the outer sublayer subsequently exchange the momentum with the ambient gas molecules after the elastic collision and collide with the middle sublayer. The material collision within the thin layer can be described as a “three-ball collision model”. Before external shock wave was produced in plasma expansion (around 150 ns [15]), the laser-induced plasma expanded with supersonic velocity and mixed with ambient gases. At the beginning of plasma expansion, the mixing process (collision between the plasma and ambient gas) is non-elastic due to the high plasma temperature. As expansion and mixing process go on, there would be a thin layer formed between the hot plasma frontier and ambient gas with very large temperature gradient, acting as the boundary layer of the plasma. Due to the existence of this thin layer, materials at two sides of the thin layer collide in different manners. Outside of the thin layer, the material is in low temperature, and the collision between

the thin layer and the ambient gas in the form of near elastic collision; while inside the thin layer, the material is in high temperature, and inner side plasma collides with the thin layer inelastically. In this way, the energy was transferred from the high plasma to thin layer as well as the surrounding gas molecules by heating the thin layer into plasma and accelerating thin layer surrounding gas and making the surrounding gas part of the thin layer. Around 150 ns, the energy and moment contained in the thin layer, inner side thin layer material, and outside thin layer reach a subtle moment, the interaction between the thin layer and outside gas generates external shockwave due to elastic collision; while the thin layer lack enough momentum to catch up the shockwave but was pushed back to the plasma to balance the force to drive the shockwave, and the inelastic collision between thin layer and the inner side material make both part move back. This is the underneath mechanism possibly explain the dash-down process. After 200 ns, the back pressed part of plasma crashed with the lower part of the plasma and subsequently flatter the plasma, ultimately split the plasma, as observed in the plasma morphological images. As said before, the crash was in so high speed and any tiny velocity make the back-pressed plasma material asymmetric would bring drastic deviation from the symmetric case. Due to inevitable loss of symmetrical back-pressed frontier material by RTI and surface roughness, the fluctuation was amplified with this dash-down and crash process, which leads to a large morphological fluctuation at later stage of plasma evolution and ultimately a large spectral signal uncertainty. This is the mechanism of the generation of plasma fluctuation and spectral signal uncertainty, which is also described in Fig. 7. In addition, similar phenomena of plasma morphological change were also observed from other samples, such as Si wafer and aluminum alloy. Further study such as the investigation of the temporal and spatial distribution of plasma species, temperature field, particle velocity field within the plasma and at the plasma frontier, will be

taken to consolidate the mechanisms of the signal uncertainty generation proposed in this work.

4 Conclusion

The mechanism of signal uncertainty generation for LIBS was investigated using temporally-resolved spectroscopic and fast-imaging plasma morphology method. Using three fast-imaging cameras to capture three consecutive images from the same laser-induced titanium alloy plasma, it was found that the plasma experienced an increasing morphological fluctuation as delay time increased, transforming from a “stable plasma” before the delay time of 100 ns to a “fluctuating plasma” after the delay time of 300 ns. Notably, the frontier part of plasma showed a significant downward motion from the delay time of 150 ns to 200 ns and collided with the lower part of the plasma, making the plasma flatter and even splitting the plasma into two parts, which was considered as a critical transformation of “stable plasma” to “unstable plasma”. By calculating the correlation coefficient of plasma image pairs at successive delay times, it was found that the tiny plasma fluctuation earlier than the critical delay time (150–200 ns) was amplified, causing a large plasma fluctuation at later stage. A possible mechanism generating plasma morphology fluctuation as well as signal uncertainty was proposed: Rayleigh–Taylor Instability (RTI) and surface roughness inevitably initiated slight plasma morphology fluctuation before 100 ns, and the generation of external shockwave (around 150 ns) back-press the plasma frontier material downwards and crash with the lower part (around 200 ns), the dash-down and crash process amplifies the slight fluctuations into large fluctuations as well as LIBS signal uncertainty. Possible initiation of the slight fluctuation at the early stage caused by RTI was also analyzed, and possible mechanism making the dash-down frontier plasma material was proposed as well.

Acknowledgements The authors thank the financial support from the National Natural Science Foundation of China (No. 61675110) and the National Key Research and Development Program Key Projects of China (No. 2016YFC0302102). We thank Patrick Hong for the paper improvement.

References

1. D. W. Hahn and N. Omenetto, Laser-induced breakdown spectroscopy (LIBS), Part I: Review of basic diagnostics and plasma–particle interactions: Still-challenging issues within the analytical plasma community, *Appl. Spectrosc.* 64(12), 335A (2010)
2. D. W. Hahn and N. Omenetto, Laser-induced breakdown spectroscopy (LIBS), Part II: Review of instrumental and methodological approaches to material analysis and applications to different fields, *Appl. Spectrosc.* 66(4), 347 (2012)
3. D. A. Cremers and L. J. Radziemski, Handbook of Laser-Induced Breakdown Spectroscopy, Wiley, 2013
4. Z. Wang, T. B. Yuan, Z. Y. Hou, W. D. Zhou, J. D. Lu, H. B. Ding, and X. Y. Zeng, Laser-induced breakdown spectroscopy in China, *Front. Phys.* 9, 419 (2014)
5. J. D. Winefordner, I. B. Gornushkin, T. Correll, E. Gibb, B. W. Smith, and N. Omenetto, Comparing several atomic spectrometric methods to the super stars: Special emphasis on laser induced breakdown spectrometry, LIBS, a future super star, *J. Anal. At. Spectrom.* 19(9), 1061 (2004)
6. J. M. Mermet, P. Mauchien, and J. L. Lacour, Processing of shot-to-shot raw data to improve precision in laser-induced breakdown spectrometry microprobe, *Spectrochim. Acta B At. Spectrosc.* 63(10), 999 (2008)
7. Z. Hou, Z. Wang, T. Yuan, J. Liu, Z. Li, and W. Ni, A hybrid quantification model and its application for coal analysis using laser induced breakdown spectroscopy, *J. Anal. At. Spectrom.* 31(3), 722 (2016)
8. E. Tognoni and G. Cristoforetti, Signal and noise in laser induced breakdown spectroscopy: An introductory review, *Opt. Laser Technol.* 79, 164 (2016)
9. X. Zeng, X. Mao, S. S. Mao, J. H. Yoo, R. Greif, and R. E. Russo, Laser–plasma interactions in fused silica cavities, *J. Appl. Phys.* 95, 816 (2004)
10. J. Yu, Q. Ma, V. Motto-Ros, W. Lei, X. Wang, and X. S. Bai, Generation and expansion of laser-induced plasma as a spectroscopic emission source, *Front. Phys.* 7(6), 649 (2012)
11. X. Bai, Q. Ma, M. Perrier, V. Motto-Ros, D. Sabourdy, L. Nguyen, A. Jalocha, and J. Yu, Experimental study of laser-induced plasma: Influence of laser fluence and pulse duration, *Spectrochim. Acta B At. Spectrosc.* 87, 27 (2013)
12. R. Wisbrun, I. Schechter, R. Niessner, H. Schroeder, and K. L. Kompa, Detector for trace elemental analysis of solid environmental samples by laser plasma spectroscopy, *Anal. Chem.* 66(18), 2964 (1994)
13. Z. Wang, Z. Hou, S. Lui, D. Jiang, J. Liu, and Z. Li, Utilization of moderate cylindrical confinement for precision improvement of laser-induced breakdown spectroscopy signal, *Opt. Express* 20(S6), A1011 (2012)
14. Z. Hou, Z. Wang, J. Liu, W. Ni, and Z. Li, Signal quality improvement using cylindrical confinement for laser induced breakdown spectroscopy, *Opt. Express* 21(13), 15974 (2013)
15. Y. Fu, Z. Hou, and Z. Wang, Physical insights of cavity confinement enhancing effect in laser-induced breakdown spectroscopy, *Opt. Express* 24(3), 3055 (2016)
16. V. N. Rai, A. K. Rai, F. Y. Yueh, and J. P. Singh, Optical emission from laser-induced breakdown plasma of solid and liquid samples in the presence of a magnetic field, *Appl. Opt.* 42(12), 2085 (2003)
17. L. B. Guo, W. Hu, B. Y. Zhang, X. N. He, C. M. Li, Y. S. Zhou, Z. X. Cai, X. Y. Zeng, and Y. F. Lu, Enhancement of optical emission from laser-induced plasmas by combined spatial and magnetic confinement, *Opt. Express* 19(15), 14067 (2011)

18. Z. Wang, Y. Deguchi, R. Liu, A. Ikutomo, Z. Zhang, D. Chong, J. Yan, J. Liu, and F.J. Shiou, Emission characteristics of laser-induced plasma using collinear long and short dual-pulse laser-induced breakdown spectroscopy (LIBS), *Appl. Spectrosc.* 71, 2187 (2017)
19. Y. Fu, Z. Hou, T. Li, Z. Li, and Z. Wang, Investigation of intrinsic origins of the signal uncertainty for laser-induced breakdown spectroscopy, *Spectrochim. Acta B At. Spectrosc.* 155, 67 (2019)
20. Z. Hou, Z. Wang, J. Liu, W. Ni, and Z. Li, Combination of cylindrical confinement and spark discharge for signal improvement using laser induced breakdown spectroscopy, *Opt. Express* 22(11), 12909 (2014)
21. X. Li, Z. Wang, Y. Fu, Z. Li, J. Liu, and W. Ni, Application of a spectrum standardization method for carbon analysis in coal using laser-induced breakdown spectroscopy (LIBS), *Appl. Spectrosc.* 68, 955 (2014)
22. X. Li, Z. Wang, X. Mao, and R. E. Russo, Spatially and temporally resolved spectral emission of laser-induced plasmas confined by cylindrical cavities, *J. Anal. At. Spectrom.* 29(11), 2127 (2014)
23. H. Yin, Z. Hou, T. Yuan, Z. Wang, W. Ni, and Z. Li, Application of spatial confinement for gas analysis using laser-induced breakdown spectroscopy to improve signal stability, *J. Anal. At. Spectrom.* 30(4), 922 (2015)
24. T. Li, S. Sheta, Z. Hou, J. Dong, and Z. Wang, Impacts of a collection system on laser-induced breakdown spectroscopy signal detection, *Appl. Opt.* 57(21), 6120 (2018)
25. S. B. Wen, X. Mao, R. Greif, and R. E. Russo, Laser ablation induced vapor plume expansion into a background gas (II): Experimental analysis, *J. Appl. Phys.* 101, 023115 (2007)
26. S. B. Wen, X. Mao, R. Greif, and R. E. Russo, Expansion of the laser ablation vapor plume into a background gas (I): Analysis, *J. Appl. Phys.* 101, 023114 (2007)
27. C. G. Parigger, C. M. Helstern, B. S. Jordan, D. M. Surmick, and R. Splinter, Laser-plasma spatiotemporal cyanide spectroscopy and applications, *Molecules* 25, 615 (2020)
28. C. G. Parigger, D. M. Surmick, and G. Gautam, Self-absorption characteristics of measured laser-induced plasma line shapes, *J. Phys. Conf. Ser.* 810, 012012 (2017)
29. S. S. Harilal, C. V. Bindhu, M. S. Tillack, F. Najmabadi, and A. C. Gaeris, Internal structure and expansion dynamics of laser ablation plumes into ambient gases, *J. Appl. Phys.* 93, 2380 (2003)
30. S. S. Harilal, G. V. Miloshevsky, P. K. Diwakar, N. L. LaHaye, and A. Hassanein, Experimental and computational study of complex shockwave dynamics in laser ablation plumes in argon atmosphere, *Phys. Plasmas*. 19, 083504 (2012)
31. V. Y. Baranov, O. N. Derkach, V. G. Grishina, M. F. Kanevskii, and A. Y. Sebrant, Dynamics and stability of an expanding laser-induced plasma in a low-density gas, *Phys. Rev. E* 8(2), 1324 (1993)
32. P. S. R. Abhilasha, P. S. R. Prasad, and R. K. Thareja, Laser-produced carbon plasma in an ambient gas, *Phys. Rev. E* 48(4), 2929 (1993)
33. A. K. Sharma and R. K. Thareja, Characterization of laser-produced aluminum plasma in ambient atmosphere of nitrogen using fast photography, *Appl. Phys. Lett.* 84, 4490 (2004)
34. D. W. Koopman, H. J. Siebeneck, and G. Jellison, Turbulent interaction fronts in counterstreaming laser-produced plasma studies, *Phys. Fluids* 22, 526, (1979)
35. A. Neogi and R. K. Thareja, Laser-produced carbon plasma expanding in vacuum, low pressure ambient gas and nonuniform magnetic field, *Phys. Plasmas*. 6, 365 (1999)
36. K. Rifai, F. Vidal, and T. W. Johnston, Theoretical investigation of the Rayleigh–Taylor instability in laser-produced plasmas driving into background gases, *Phys. Plasmas*. 14, 082311 (2007)
37. R. A. Marin, C. A. Gonzales, and H. Riascos, Rayleigh–Taylor analysis in a laser-induced plasma, *J. Phys. Conf. Ser.* 370, 012063 (2012)
38. H. J. Kull, Theory of the Rayleigh–Taylor instability, *Phys. Rep.* 206(5), 197 (1991)
39. L. J Radziemski, *Lasers-Induced Plasmas and Applications*, Taylor & Francis, 1989
40. T. Lü, Y. Hu, J. Meng, Z. Li, C. Zhang, X. Zhang, and E. Tuyizere, Secondary shock wave: Implication for laser ablation inductively coupled plasma mass spectrometry, *J. Appl. Phys.* 124, 073101 (2018)
41. B. Campanella, S. Legnaioli, S. Pagnotta, F. Poggialini, and V. Palleschi, Shock waves in laser-induced plasmas, *Atoms* 7(2), 57 (2019)